Ab initio and experimental studies of chlorine adsorption on the rutile TiO_2 (110) surface

Doris Vogtenhuber* and Raimund Podloucky
Department of Physical Chemistry, University of Vienna, Liechtensteinstrasse 22a/I/3, A-1090 Vienna, Austria

Josef Redinger
Department of Solid State Theory, University of Technology of Vienna, Getreidemarkt 9/158, A-1060 Vienna, Austria

Eleonore L. D. Hebenstreit, Wilhelm Hebenstreit, and Ulrike Diebold
Department of Physics, Tulane University, New Orleans, Louisiana 70118
(Received 29 August 2001; published 13 March 2002)

We report a comprehensive study on the adsorption of Cl on the clean rutile TiO_2 (110) (1×1) surface. STM and photoemission spectroscopy results are compared to *ab initio* results. At room temperature, Cl adsorbs dissociatively and binds to the fivefold coordinated Ti atoms in an on-top configuration. The calculations predict energetically more favorable adsorption on a reduced surface, where bridging oxygen atoms are missing in a (1×4) geometry. Experimental photoemission data indicate a quenching of the oxygen-vacancy-related defect state upon chlorine adsorption at room temperature, in agreement with the theoretical results. Chlorine atoms appear as bright, extended spots in experimental empty-states STM images. Calculations of density-of-states contours indicate that Ti states underneath the Cl atoms are predominantly responsible for the tunneling current. When chlorine is dosed onto a hot surface, a replacement of bridging oxygen atoms is observed in addition to features of unidentified structure and stoichiometry. The experimental results on the change in work function and shift of Cl core levels agree semiquantitatively with calculations of different test geometries.

DOI: 10.1103/PhysRevB.65.125411 PACS number(s): 68.43.Bc, 68.43.Fg, 68.35.−p, 68.37.Ef

I. INTRODUCTION

Adsorption processes on well-characterized metal oxide surfaces are of considerable practical and fundamental interest. Amongst all the single-crystalline metal oxides, the TiO_2(110) surface has been studied most extensively with theoretical[1–6] as well as experimental[7–12] techniques, and the geometric, electronic, and defect structure is very well understood. It is thus a good model substrate to undertake model studies of the surface reactivity at the molecular level. In this paper, a simple, diatomic molecule Cl_2 has been chosen as a test molecule. Chlorine is a common impurity in polycrystalline powder materials, and its presence is known to affect reaction processes.[13] Thus, a detailed knowledge of adsorption geometries and adsorption-related effects on the electronic structure might be interesting from an applied view as well.

This paper is part of a series of recent publications on electronegative adsorbates. The adsorption of S is treated in Refs. 14–17 and the dissociation and adsorption mechanisms of Cl_2 have been discussed in Ref. 18. This paper combines experimental investigations with detailed *ab initio* calculations. The experimental results are discussed in more detail in Ref. 19, and only the most relevant results are summarized here.

It is widely accepted that defects on metal oxide surfaces are reactive sites.[20] Local nonstoichiometries and other imperfections change both, the surface geometric and electronic structure. Local probes such as scanning tunneling microscopy (STM) are very well suited to study defect-related adsorption and reaction mechanisms[18,21,22] and can give a first impression of adsorption sites and mechanisms. However, because the STM image contrast is largely dominated by electronic structure effects,[9,23,24] interpretation of STM images is often not straightforward. The combination of first-principles total-energy calculations with STM measurements and area-averaging spectroscopic techniques is thus a promising approach to obtain a very detailed picture of adsorbate structures. In addition, it allows insight into the STM imaging contrast of adsorbates on a metal compound surface with a strongly varying local electronic structure.

II. EXPERIMENTS

A. Experimental details

The experimental setup and procedure have been discussed in more detail in Refs. 14–17,19. A clean, (1×1) surface with a small density of point defects (vacancies in the bridging oxygen rows) was prepared as described previously. All STM results shown are empty-states images acquired at room temperature with the sample biased and the tip held close to ground potential. Photoemission spectroscopy of core levels was performed with a dual-anode x-ray source. Valence band (VB) spectra were taken with synchrotron-based radiation at the Center for Advanced Microstructures and Devices. The molecular chlorine was produced by electrolytical dissociation of AgCl in an ultrahigh-vacuum compatible cell.[25] Results are reported after adsorption on the clean surface (containing the O vacancies) at room temperature and at 200 °C–300 °C. A stoichiometric substrate (as judged by photoemission) was produced by adsorbing molecular oxygen at room temperature before exposure to chlorine. The coverages were estimated using a combination of x-ray photoemission spectroscopy (XPS) and STM[19] and are

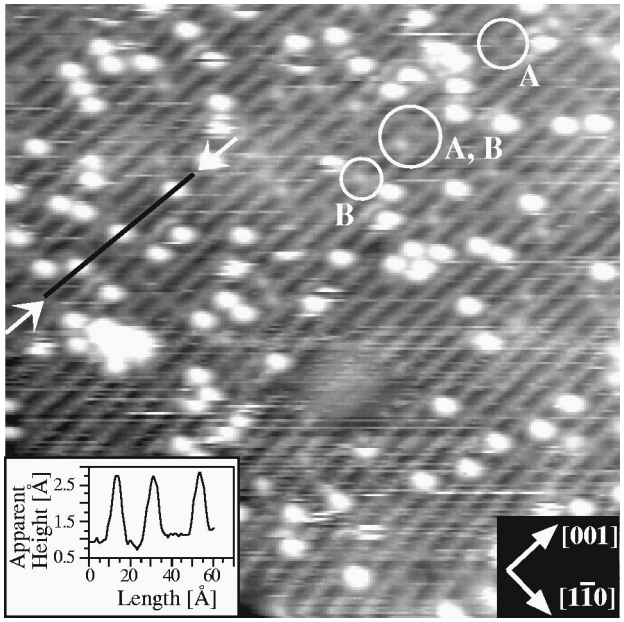

FIG. 1. An STM image (200 Å×200 Å, +1.4 V, 0.4 nA) after Cl adsorption at room temperature. Each bright spot, located on light gray row, represents a single Cl atom adsorbed on a $Ti^{[5]}$ atom. The apparent height of the Cl atoms is indicated in the line scan. Two kinds of light spots, labeled with *A* and *B*, respectively, are located at the dark oxygen rows. Possibly, type *A* represents bridging oxygen vacancies and type *B* represents oxygen vacancies filled with Cl.

given in monolayers (with 1 ML=1 Cl atom per surface unit cell). Work function changes have been measured by comparing the position of the low-energy cutoff of the secondary electron spectrum on the biased sample. No attempt has been made to determine the absolute value of the work function.

B. Experimental results

The STM image in Fig. 1 shows a TiO_2 (110) surface with a small coverage of Cl, adsorbed at room temperature. In agreement with previous STM results of Cl/TiO_2,[18,19] the chlorine atoms appear as bright spots located on the light gray rows that are generally accepted as being representative of the fivefold coordinated Ti atoms ($Ti^{[5]}$) at the surface. The Cl features are large and exhibit an apparent height of 2 Å above the titanium rows. No long-range ordering of the adsorbate is visible at any coverage. Some streakiness in the images as well as Cl atoms that appear ''cut'' indicate some mobility at the given tunneling conditions. Indeed, scanning with a higher bias voltage (not shown here) can clear off the Cl from the surface, or can push single Cl atoms along the $Ti^{[5]}$ rows during consecutive scans.

The substrate surface has been prepared by sputtering and annealing in ultrahigh vacuum (UHV), which typically results in a few percent of vacancies in the bridging oxygen rows. This is also apparent in the valence band photoemission spectra [Fig. 2(a)] of such a surface. The presence of oxygen vacancies on the TiO_2 (110) surface leads to an excess of electrons in the neighborhood of the defects which populate a state within the band gap.[20,26–28] This defect state

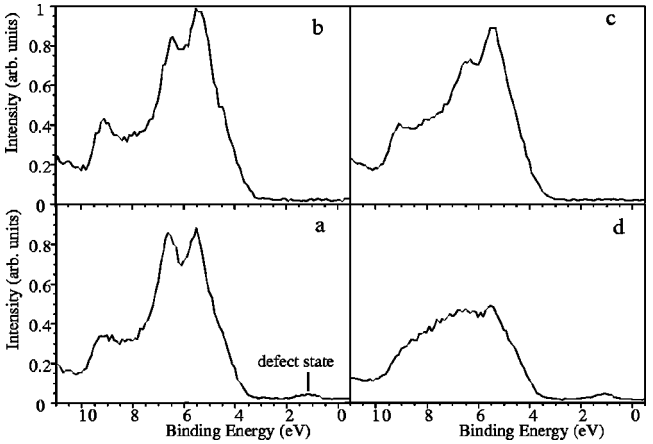

FIG. 2. Photoelectron spectra (normal emission, $h\nu=40$ eV) of the valence-band region from (a) the clean TiO_2 (110) surface containing point defects; (b) after dosing of oxygen at room temperature; (c) with a saturation coverage of Cl, adsorbed at room temperature on the surface described in (b); and (d) after exposure to Cl_2 at 200 °C. The spectra have been normalized to the photon flux.

disappears upon exposure to molecular oxygen at room temperature [Fig. 2(b)]. Dissociative adsorption of the oxygen molecules results in a filling of the oxygen vacancies.[29] The upper edge of the VB is shifted to lower binding energy by 0.2 eV. The spectrum in Fig. 2(c) is representative for Cl adsorbed at room temperature on either a slightly defective surface or on one that has been predosed with oxygen. In both cases the defect state disappears. The shapes of the spectra in Figs. 2(a)–(c) are remarkably similar, with only the relative intensities of the main peaks somewhat altered.

It is well accepted that defects in the bridging oxygen rows appear as bright spots on dark rows on TiO_2 (110).[9,23,24] Upon adsorption of Cl on such a slightly defective surface, both faint and somewhat brighter spots appear at the dark bridging oxygen rows. Representative features are marked with the white circles *A* and *B* in Fig. 1. The large circle points out two of these different spots next to each other. Based on the theoretical results discussed below, and consistent with the quenching of the VB defect state upon Cl adsorption in Fig. 2, we interpret one of these spots as a Cl atom filling an oxygen vacancy.

The adsorption geometry changes considerably when Cl_2 is dosed on a hot surface (200 °C–300 °C), see Fig. 3. The bright spots, indicative of single Cl atoms, are now centered on the dark rows, i.e., at the position of the bridging oxygens. Their number increases with increasing coverage. In addition, ca. 15-Å-wide and several angstroms high protrusions form. Neither the internal structure nor the exact stoichiometry of these protrusions could be determined with the experimental techniques applied in this work. It is likely that they contain several Cl atoms.[19] Stable TiOCl and $TiOCl_2$ compounds have been described in Refs. 30,31, respectively. It is well possible that these surface features resemble these structures to some extent. The Cl 2*p* level is shifted to higher binding energies by 0.4 eV compared to the value of 199.4 ±0.1 eV for adsorption at room temperature. The valence band spectrum from such a surface is considerably changed,

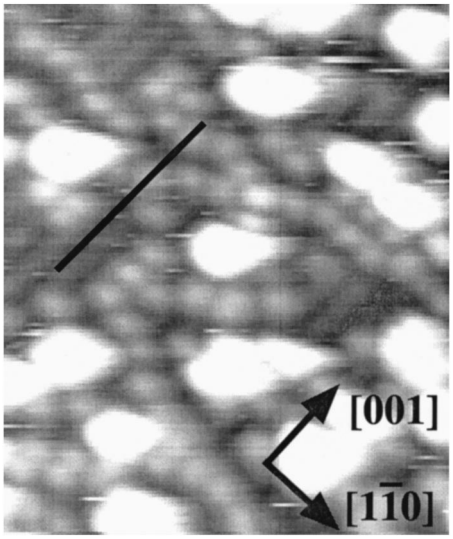

FIG. 3. An STM image after adsorption of 0.25 ML Cl at 200 °C. The light gray spots in registry with the dark substrate rows (the bridging oxygen atoms) are identified at Cl substituting O atoms. In addition, larger protrusions appear upon Cl adsorption with unidentified structure and stoichiometry.

see Fig. 2(d). A pronounced defect state appears, and the features of the valence band appear smeared out. The total intensity of the spectrum is smaller. In Ref. 19 it is argued that the small cross section of photoemission from the Cl $3p$ levels[32] causes the reduction in signal intensity in these surface-sensitive measurements. The pronounced defect state is also reflected in XPS measurements of the Ti $2p$ peak. A stoichiometric surface contains Ti atoms in a (formally) Ti^{4+} oxidation state while the oxygen atoms are (formally) O^{2-} anions. A surface with a few percent of oxygen vacancies [Fig. 2(a)] exhibits a Ti^{3+} shoulder, which typically constitutes 2% of the Ti $2p_{3/2}$ peak in these experiments. This shoulder increases by a factor of 2 after adsorption of 1.2 ML Cl at 300 °C.[19] The increase scales with the density of single Cl atoms replacing bridging oxygens rather than the number of the larger protrusions.

The change in work function has been measured for the different surfaces. Taking the clean, slightly defective surface as a reference, chlorine adsorption results in an increase of the work function by 0.7 eV and 0.5 eV for adsorption at room temperature and 200 °C, respectively. The adsorption of oxygen on the slightly defective surface results in a work function increase by 0.8 eV. One has to be careful with interpreting this latter value, however, as a small amount of hydroxyls could have been present on the oxygen-dosed surface. Because water adsorption is precursor mediated,[33] it happens much more rapidly than the dissociation of oxygen molecules at the oxygen vacancies. It is well possible that a trace amount of water is contained in the oxygen gas when the ultrahigh vacuum chamber is backfilled during the O_2 exposure. Thus, some of the surface oxygens could possibly be hydroxylated, changing the work function value considerably.

Understanding the image contrast of adsorbates in STM is one focal point in this paper. Normally, STM images of

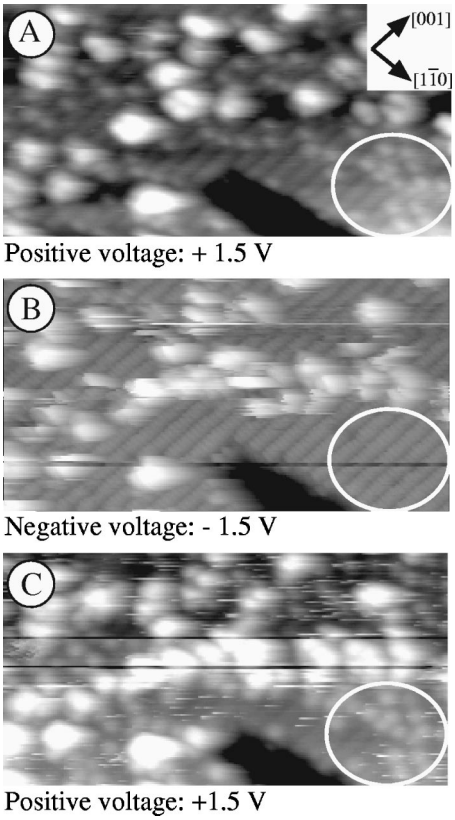

FIG. 4. STM sequence (200 Å×200 Å, I_t=0.3 nA) after adsorption of Cl at 200 °C with different tunneling voltage polarities.

filled-state images are of poor quality, if feasible at all. The bands in the O $2p$ region are rather flat,[34] and the hole conductivity is small. In addition, the Fermi level is located at the lower edge of the conduction band in the (intrinsically *n*-type doped) bulk. This necessitates a high bias voltage to bridge the 3 eV gap and causes an often unstable tunneling junction. When the surface was exposed to Cl at high temperature, filled-state images with satisfactory quality could be obtained (Fig. 4). Interestingly, the single Cl atoms are not visible in filled-state images, see Fig. 4(b). A consecutive image with positive bias shows that no Cl is removed during the scan and that the atoms are largely at the same positions, see the circles in Fig. 4.

III. CALCULATIONS

A. Computational details

The *ab initio* calculations were performed applying the full potential linearized augmented plane wave (FLAPW) method,[35] based on density functional theory (DFT, Ref. 36), in its version for free single slabs. We chose the local density approximation (LDA) in the parametrization of Hedin and Lundqvist.[37] The wave-function cutoff of the augmented plane waves was 4.1 a.u.$^{-1}$, corresponding to approximately 180 basis functions per atom. Within the atomic spheres, the angular parts of density and potential were expanded up to $l_{max}=6$ (Ti) and $l_{max}=4$ (Cl and O), respectively. Two general $\vec{k}$ points within the irreducible part of the two-

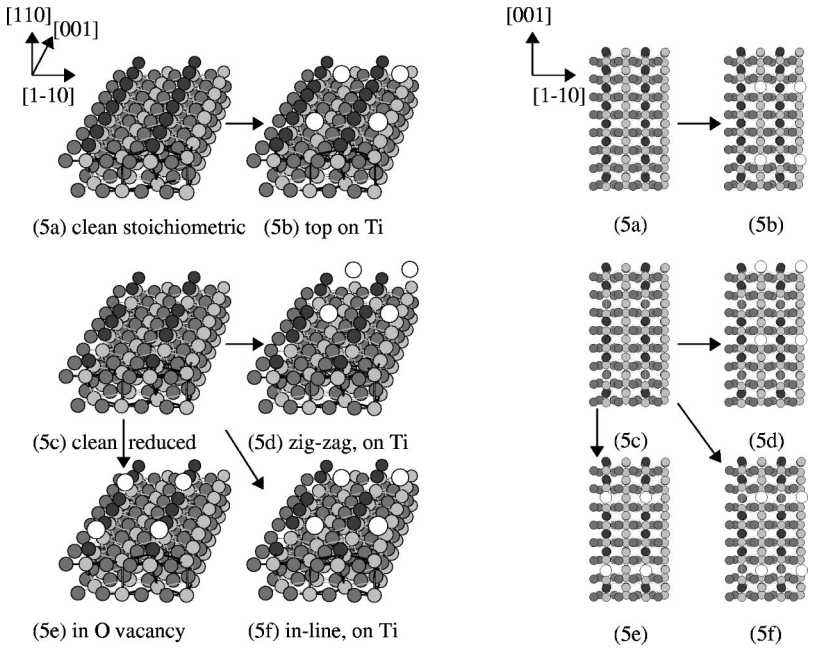

FIG. 5. Model adsorption geometries of Cl adsorption on the stoichiometric and reduced rutile-TiO_2 (110) surface. Small black circles: bridging O, small dark-gray circles: all other O; small light-gray circles: Ti, large white circles: Cl. Only the upper part of the slab is shown. Figures 5(a),(c) show the clean substrates, Figs. 5(b),(d),(e),(f) the Cl-adsorbed slabs. For details see text.

dimensional Brillouin zone (IBZ) were used to obtain self-consistency of the charge densities. The Brillouin-zone integrations were performed by triangular integration over a regular mesh of 25 $\vec{k}$ points in the IBZ.[38]

The experimental lattice parameters ($a=4.593$ Å, $c/a=0.664$) of rutile TiO_2 were taken for the geometry setup. A more extensive description of the computational details will be given elsewhere.[39]

All surfaces were modeled by free single slabs with a thickness of three TiO_2 formula units. Equilibrium geometries, adsorption energetics, electronic structures, and STM images were calculated for several model adsorption geometries, which are summarized in Fig. 5. The relaxed geometries were calculated by minimization of the forces[40,41] on all atoms in and above the mixed surface plane, which were allowed to relax under the constraint that the *pmm* symmetry of the unit cell is not broken.

In the present study, (1×4) superstructures (corresponding to vacancy densities and adsorbate coverages of $\frac{1}{4}$ ML, respectively), were chosen for the O-defective and the Cl-adsorbed slabs. Results on high-coverage adsorbate densities, modeled with (1×2) supercells, will be discussed in a forthcoming paper. These higher-coverage adsorption types are energetically less favorable for all assumed model geometries,[39,42] in good agreement with experiment, where a saturation coverage of 0.3–0.4 ML is found.[18,19] For the study of adsorption on the stoichiometric substrate surface (upper panels in Fig. 5), on-top adsorption on the undercoordinated $Ti^{[5]}$ atoms [Fig. 5(b)] was considered, because this geometry was shown to be slightly more stable than a bridging adsorption type for the (1×2) high-coverage limit.[42] In our model structure of the reduced substrate (lower panels of Fig. 5), every fourth of the bridging O atoms was missing [Fig. 5(c)], which results in a variety of adsorption sites. To investigate the influence of the nearest and next-nearest neighbors, we considered three different adsorption geometries. In the first one Cl fills an O vacancy [Fig. 5(e)], corresponding to the high-temperature adsorption type of the experiment, as shown in Fig. 2 and Fig. 3. In this geometry, Cl–O–O–O–Cl chains are formed along the [001] direction. In addition, Cl may again be bound to one of the $Ti^{[5]}$ atoms, comparable to adsorption on the stoichiometric substrate, and predominantly present at low temperatures, see Fig. 1. Considering the latter case, we compared adsorption on two nonequivalent $Ti^{[5]}$ sites, either adjacent to, or in maximum distance from an O vacancy ○ [Figs. 5(f) and 5(d), respectively]. These adsorption types are referred to as ''in-line'' and ''zigzag'' adsorption types further on. The two structures differ with respect to the next-nearest neighbors along the $[1\bar{1}0]$ direction. Either chains of –○–Cl–○–Cl– or chains of –O–Cl–O–Cl– are formed due to the periodicity of the slab.

STM images were calculated based on the Tersoff-Hamann model[43] by which the local vacuum DOS (density of states) serves as a first approximation for the image contrast. In this model the STM tip is described by a *s*-type wave function, tip-substrate interactions are neglected and the tunneling process is treated within a perturbational approach. Hence the tunneling current is proportional to the charge density of sample states at the position of the tip apex atom, which satisfy elastic tunneling conditions corresponding to the applied tip-sample bias voltage. The charge-density contours of the empty-states DOS were calculated according to the experimental tip polarity. Despite the substantial approximations made in the Tersoff-Hamann model, this approach worked satisfactorily for the clean rutile (110) surface.[9,24] Predominantly empty-states images were acquired experimentally on the *n*-type semiconducting TiO_2 crystals. In approximation to the experimental parameters, the calculated DOS was integrated up to an energy of 1.6 eV above conduction band minimum.[23]

The transition matrix elements of the calculated valence-band photoelectron spectra (VB-PES) were calculated within the single-scatterer final-state approximation.[44] Thus, the cal-

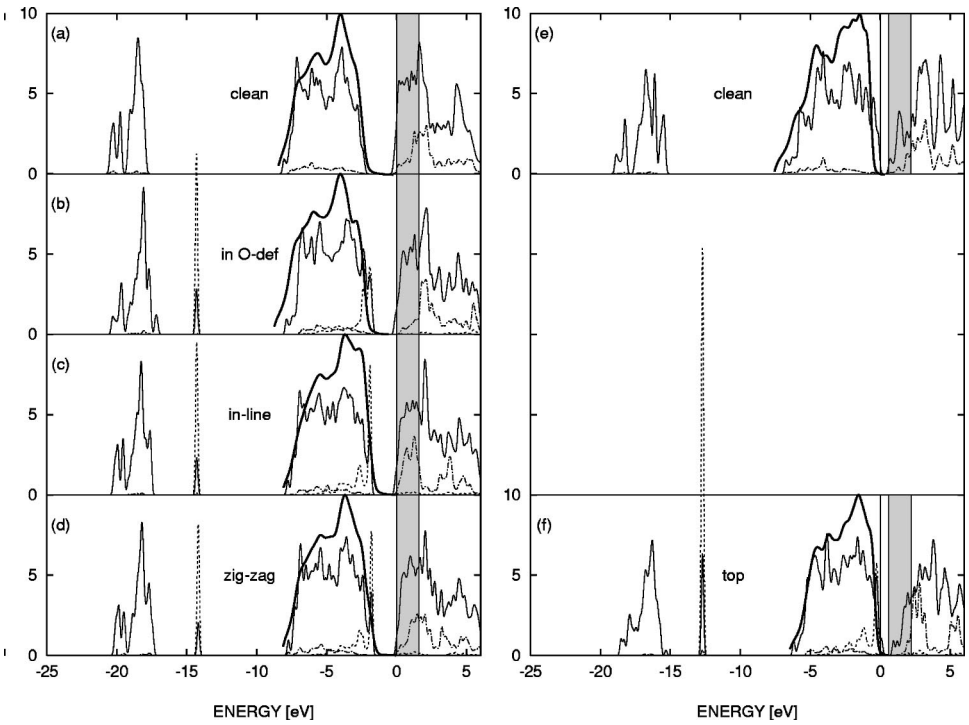

FIG. 6. Densities of states (DOS) and calculated photoelectron spectra (VB-PES) of the clean and Cl-adsorbed rutile surfaces in states/eV. Left panels: reduced substrate surface, right panels: stoichiometric substrate surfaces. Bold full lines correspond to the VB-PES, full lines give the total DOS, divided by ten. Dotted lines: partial Cl-DOS, and dashed-dotted lines: partial Ti-DOS of the Ti atom responsible for the STM tunneling current (in DOS/atom). The gray-shaded boxes: energy region of the states that contribute to the tunneling current.

culated spectra, shown as a solid bold line in Fig. 6, may be viewed as a cross-section-weighted average of the local partial DOS (LDOS), with cross sections calculated from ''atoms'' in the solid. According to experiment,[17] the photon energy, and spectrometer resolution were set to 40.8 eV and 0.35 eV, respectively. A Lorentzian lifetime broadening of 0.07 eV was assumed for the initial states. Finite lifetimes effects of the outgoing photoelectrons due to unspecific multiple scattering processes determine mostly the escape depth and may be translated roughly into a *z*-dependent decay factor of the signal intensity. Outgoing electrons originating from atoms further away from the surface contribute less to the total PES signal. Omitting these effects as done in our calculation for TiO_2 artificially enhances the contributions of subsurface atoms that dominate the LDOS near the lower *p*-band edge. Two assumptions in the single-scatterer final-state approximation that need some attention are (i) the neglect of the surface barrier in the emission process and in the final-state wave functions, and (ii) the neglect of $\vec{k}$ conservation. Both assumptions are certainly well met for high photon energies such as in the XPS regime, but become less justified when approaching the traditional ultraviolet photoemission spectroscopy (UPS) regime ($h\nu = 40.8$ eV). However, as the surface barrier is only neglected in the final state, and since the potential varies smoothly in the surface region, assumption (i) would only introduce larger errors if the final state would be pinned to the surface region by a bulk energy gap for that particular energy range. The largest effect of the surface barrier is certainly on the energetic positions of those initial states protruding far out into the vacuum, which are correctly treated by the FLAPW free slab surface barrier.[45] Assumption (ii) certainly seems to be a rather crude approximation for typical UPS photon energies, such as in the present case, where direct $\vec{k}$ conserving transitions should constitute the main part of the photocurrent. Nevertheless, it is less severe than supposed at first guess, because performing the angular averaging is rather helpful. All regions of $\vec{k}$ space are probed for the photon energies used and the energy dependence of the single-scatterer cross sections is taken into account in a $\vec{k}$-averaged way. So it is mainly the $\vec{k}$ dependence of the cross sections due to particular orbital symmetry dependent selection rules, which is neglected in our approach. Consequently states along high-symmetry directions will be affected most, and their contribution is overstated in the calculated PES.

B. Computational results

1. Relaxations and bondlengths

The calculated equilibrium geometries of clean and adsorbate-covered substrate films show considerable changes in relaxations and bond lengths upon Cl adsorption (see Table I). As details of the equilibrium geometries will be given elsewhere,[39] only the main effects of adsorption are summarized here.

On the clean stoichiometric and reduced substrate surfaces, relaxations shorten the remaining bonds of atoms that lost coordination partners upon surface formation. This is mainly accomplished by strong inwards relaxations of the undercoordinated Ti atoms ($Ti^{[5]}$) and the bridging O atoms, which form the outermost rows of atoms along [001]. Furthermore, minor changes occur of the positions of the surface Ti atoms ($Ti^{[6]}$) below the bridging O, and the O atoms that lie in the surface plane, O(plane), which move slightly outwards (Ti, O) and laterally (O).[46] Upon reduction of the surface, the Ti atoms adjacent to the O vacancy also become undercoordinated and these atoms move closer towards their bulk O neighbors, denoted by O(3).

TABLE I. Bond lengths in Å. From left to right: increasing distance from the adsorbate. The geometries are ordered with respect to decreasing stability for each adsorption type. For in-line geometries on the reduced substrate surface, the $Ti^{[6]}$ atoms next to the O vacancy are also adjacent to the Cl on the $Ti^{[5]}$ rows, which is not the case for the zigzag geometries. See also Fig. 5.

	Cl–Ti	$Ti^{[5]}$–O(2)			$Ti^{[6]}$–O(b.)		$Ti^{[6]}$–O(3)	
Stoichiometric substrate								
Clean		1.73	1.73	1.73	1.75	1.75	1.98	1.98
$Ti^{[5]}$	2.16	1.94	1.73	1.75	1.67	1.71	1.77	1.92
Reduced substrate								
Clean		1.68	1.69	1.69	1.72	1.72	1.63	1.94
$\bigcirc^{O}$	2.43	1.67	1.68	1.69	1.68	1.71	1.71	1.93
$Ti^{[5]}$,*i.-l.*	2.20	1.86	1.67	1.69	1.67	1.70	1.58	1.93
$Ti^{[5]}$,*z.-z.*	2.18	1.91	1.67	1.69	1.71	1.70	1.93	1.60

Adsorption of Cl has mainly two effects on the substrate surfaces considered.

(i) When undercoordinated TiO_2 surface atoms become bound to the Cl atoms, they regain their bulklike coordination. Therefore, the large relaxations found at the clean surfaces are (partly) lifted, as can be seen by close inspection of Fig. 5 and Table I. For all adsorption types where Cl binds to $Ti^{[5]}$, the $Ti^{[5]}$ atoms move considerably outwards with respect to their positions on the clean substrate surfaces. This results in weakened bonds between the Ti atoms and the O atoms in the layer underneath, denoted O(2) atoms. If Cl is adsorbed in a vacant O site, the bonds to the neighboring atoms become very similar to the stoichiometric surface.

(ii) The strongly electronegative Cl atoms push away the oxygens. However, these effects are very short ranged and therefore restricted to the nearest oxygen atoms only. If Cl is adsorbed in a vacancy in the bridging O rows, it is located slightly above the O atoms in the rows. Upon adsorption on top of a $Ti^{[5]}$ on the stoichiometric surface, the bridging O in registry with Cl shows a stronger inwards relaxation compared to the neighboring O [see Fig. 5(b)]. On the reduced surface the positions of the bridging O are generally closer to those in the bulk for the considered (very high) vacancy concentrations, making the influence of Cl adsorption less pronounced. As mentioned above, significant changes in bond lengths are found only for atoms directly involved in adsorbate-substrate bonding. Therefore, the Ti–Cl bond lengths are almost independent of adsorbate coverage density[39] and the stoichiometry of the substrate surface. The shortest bond lengths (2.2 Å) are found for singly bound Cl atoms on $Ti^{[5]}$, irrespective of the surface stoichiometry [see Figs. 5(b),(d),(f) and Table I]. If Cl is adsorbed along the bridging O rows, the Ti–Cl bonding distances of the $Ti^{[6]}$–Cl–$Ti^{[6]}$ are slightly larger (2.4 Å) because the Cl atoms are pushed towards the vacuum by the electronegative O neighbors [see Fig. 5(e)]. The largest Ti–Cl bond lengths of 2.8 Å are found if Cl is in a bridging position between the undercoordinated $Ti^{[5]}$.[42] This adsorption type is energetically least favorable[42] (though clearly stable) and should be regarded as a transition state of Cl as it diffuses along the Ti rows.[18] Judging from other Cl-adsorption systems,[47] one would expect an increase of the Cl–Ti bond length of about 2% upon replacing the LDA-V_{xc} by generalized gradient approximation (GGA).

TABLE II. Adsorption energies E^{ads}, $Cl_{2p_{3/2}}$ core level energies, gap widths ΔE_{gap}, *p*-band widths $\Delta E_{p-\mathrm{bd.}}$, and work functions φ of the studied adsorption geometries. All values are given in eV.

	E^{ads}	$E(\mathrm{Cl}_{2p_{3/2}})$	ΔE_{gap}	$\Delta E_{p-\mathrm{bd.}}$	φ
Stoichiometric substrate					
Clean			0.66	6.74	7.16
Top ($Ti^{[5]}$)	−2.71	−189.94	0.13	7.37	7.38
Reduced substrate					
Clean			2.06	5.81	5.16
$\bigcirc^{O}$	−5.62	−189.59	1.50	6.25	6.10
$Ti^{[5]}$,in-line	−5.35	−189.57	1.63	6.63	6.10
$Ti^{[5]}$,zigzag	−5.21	−189.44	1.64	6.06	5.98

2. Energetics

The *adsorption energies* E^{ads}, given in Table II were calculated by taking the difference of the total energies *E* of the totally relaxed final (Cl-adsorbed surface) and initial states (clean substrate surfaces + Cl atoms):

$$E^{ads}=\frac{1}{2}[E(\mathrm{Cl/TiO}_{2-x})-E(\mathrm{TiO}_{2-x})-2E(\mathrm{Cl})] \quad (1)$$

For the stoichiometric substrate surface, $x=0$. As the free slab has two equivalent surfaces, the factor of $\frac{1}{2}$ provides that all energies are given as total energy per surface. Compared to the adsorption energies of (1×2) Cl-adsorbed TiO_2,[39,42] a lower coverage is favorable for all considered model geometries. Furthermore, the calculated adsorption energies show that the O vacancy is the most active adsorption site. In general, the adsorption energies are substantially larger if Cl is adsorbed on the reduced rutile substrate surface. The calculated dissociation energy of Cl_2 (1.71 eV/Cl atom at 0 K) is included in the energy balance. This value is considerably larger than the experimental value of 1.25 eV/atom (at 298 K),[48] due to the temperature difference between calculation and experiment, and to the well-known feature of the overestimation of bond strengths by LDA calculations. If, again, the GGA was used instead of LDA, we expect that the Cl–Ti overbinding would be reduced by 15%.[47]

For free slab geometries, the zero level of potential and energy is naturally given, $\lim_{z\to\infty}V=0$. Therefore, work functions φ (Table II) correspond to the energies of the highest occupied level with respect to the vacuum zero. The calculated changes in φ vary little with Cl coverage but quite considerably with the substrate surface stoichiometry.[39]

3. Electronic structure

The DOS were calculated for the relaxed slabs. Figure 6 displays the total DOS (full lines, divided by a factor of 10) the partial Cl-DOS (dotted lines), and the partial DOS of the Ti atoms involved in the Cl bonding (dashed-dotted). The left and right panels show the DOS of reduced and stoichio-

metric substrates, respectively. The gray-shaded box depicts the energy range over which the states contributing to the STM tunneling current were sampled (from E_F to +1.6 eV). The data of *p*-band widths and gap widths are given in Table II.

The DOS of clean $TiO_{(2-x)}$ surfaces is split into occupied O *s* and *p* bands, and the predominantly Ti $3d$-derived Ti band that is separated from the O states by a gap [Figs. 6(a),(e)]. The energies of the O $2s$ states are typically 18 eV−15 eV below the valence band maximum, irrespective of the substrate stoichiometry and the presence of Cl adsorbates. The O $2p$ bandwidth is about 5.8−6.7 eV (see Table II) and in good agreement with the experimental spectra in Fig. 2. The calculated width of the fundamental gap strongly depends on the presence of O vacancies. Stoichiometric TiO_2 is a semiconductor with an experimental gapwidth of 3 eV. However, as DFT is a ground-state theory, the energies of the unoccupied Ti *d*-band levels are not calculated reliably. Therefore, the calculated gapwidth ($\approx$0.7 eV, see fourth column of Table II) has no physical meaning and is far too low. However, as the surface becomes reduced, the lowest levels of the Ti *d* band become occupied and therefore, states at both edges of the gap are occupied even in the ground state. As a consequence, the calculated gapwidth increases significantly. Because the gap state found in experiment is incorporated into the lower edge of the conduction band, the gapwidth still is too low by about 0.9 eV.

The adsorption of Cl induces additional states. A sharp Cl $3s$ peak is found $\approx$3 eV above the O *s* band. The position and *E* dispersion of the Cl $3p$ states depend on the local environment of the adsorbate. If Cl is singly bound to an undercoordinated $Ti^{[5]}$ atom, a sharp peak appears at the upper edge of the O *p* band.

The width of the *p* band is increased by 0.5–0.8 eV, corresponding to the width of the additional Cl *p* peak at the upper edge of the VB. However, the shape and energetic position of this Cl peak is independent of the substrate surface stoichiometry, as can be seen by comparison of Figs. 6(c),(d),(f) and Cl-coverage density.[39] If Cl is close to O atoms, as in the new Cl adsorption type [Fig. 6(b)], the states are distributed over the whole *p* band, due to interaction with the O states.

The partial DOS at the upper valence band edge shows significant differences in the characteristics, depending on the adsorption type of Cl. The uppermost VB states of the clean stoichiometric and reduced surface show bridging O and subsurface O(3) character, respectively. If Cl fills an O vacancy, Cl *p* and O(3) *p* states (of the oxygen seated below Cl) contribute to the VBM-DOS. On the other hand, if Cl is bound to $Ti^{[5]}$, the four uppermost VB states are derived from Cl only. Most probably these states correspond to p-[001] and p-[$1\bar{1}0$] orbitals, because the p_z states (p-[110]) lie at higher binding energies, due to the strong interaction with $Ti^{[5]}$-d_{z^2}. Upon adsorption on $Ti^{[5]}$ on the stoichiometric surface, E_F shifts from the valence band maximum to lower values. Each Cl atom contributes three *p* states but only five electrons, thus rendering empty levels at the upper edge of the VB. An analysis of the partial DOS (not shown in detail) shows that this empty state is derived from a subsurface O(3) atom next to $Ti^{[6]}$. However, it should be pointed out that these differences in the adsorption-type-dependent VBM characteristics and E_F positions are strongly related to our model geometries, which assume a 1:1 ratio of O vacancies and Cl adsorbates. This leaves the highest VB peak empty upon Cl adsorption on the stoichiometric surface and the lowest CB states occupied in all structures involving O vacancies. A Cl:O-vacancy ratio of 2:1 would, for example, pin E_F exactly at the valence band edge, as for the clean stoichiometric surface.

The shape of the calculated photoelectron spectra differs significantly from the total DOS, as can be seen from Fig. 6. The differences arise from the relative sizes of the atomic transition matrix elements and their respective energy dependences. For all considered model geometries, the O $p \rightarrow (s,d)$ transition matrix elements are bigger by a factor of ca. 5 than the Ti $d \rightarrow (p,f)$ and the Cl $p \rightarrow (s,d)$ matrix elements. Moreover, their magnitudes decrease significantly (30% for O and 50% for Ti and Cl, respectively) with increasing binding energies. Therefore, although the positions of the peaks coincide in DOS and PES, the intensities of the spectra decrease towards the *p*-band minimum whereas the height of the DOS peaks is almost constant over the whole energy range.

4. Ab initio simulation of STM images

As already mentioned in Sec. III A, STM images were simulated within the Tersoff-Hamann approach. Figures 7 and 8 display the contour lines of the unoccupied states along [001]. The bold lines are at the position of 5 Å above the surface, in rough correspondence with an expected experimental tip-sample distance. A maximum along a given contour line corresponds to a maximum in the STM corrugation, which is seen as a bright spot in a measured STM image. Only cuts along the $Ti^{[5]}$ and bridging-O rows are plotted as there are no additional corrugation maxima normal to these lines. A rough estimate of the differences in corrugation along [$1\bar{1}0$] can be made by comparing the upper and the lower panels in each of the figures.

As seen from Fig. 7, Cl adsorbed on $Ti^{[5]}$ should always appear as a bright, extended spot. The broad maxima of the contours are spread over about three unit cells along [001], which would make it impossible to determine the exact position of the adsorbate atom on the Ti rows in STM. The shape and extension of the calculated corrugation maxima are almost independent of the presence of vacancies in the neighboring O rows, as can be seen from the three panels in the upper part of Fig. 7. Moreover, Cl features also extend to the neighboring O rows. The bridging O rows remain darker compared to the adsorbate features, as for the clean surfaces. Although all bridging O are (almost) equivalent, the region next to Cl appears brighter. This effect is even more striking when Cl is adsorbed on $Ti^{[5]}$ in zigzag geometry in maximum distance to the vacancy (right panel in the bottom part of Fig. 7). Usually, O vacancies appear as bright spots along the dark O rows,[23] see circles in Fig. 1. However, an adsorbed Cl atom makes the neighboring O appear brighter

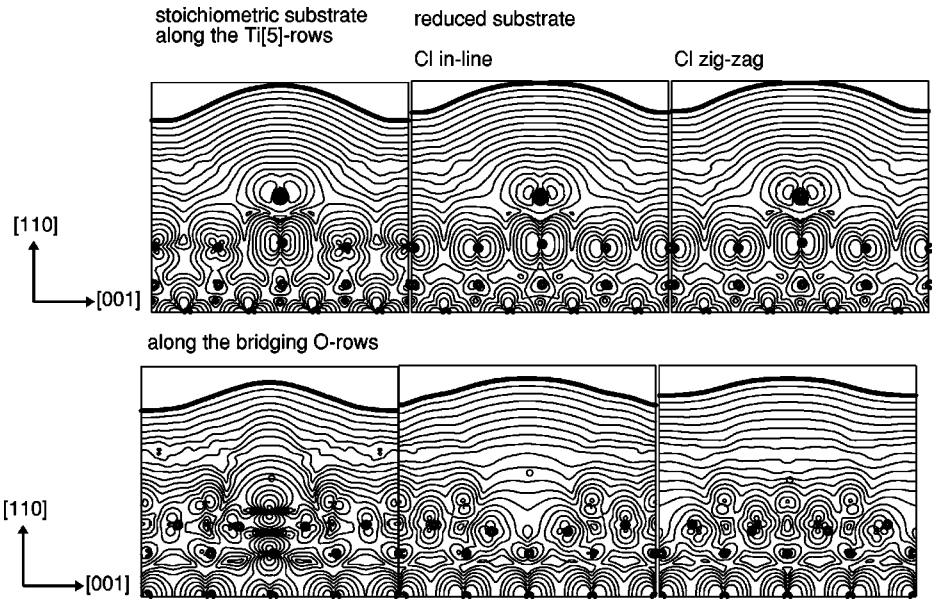

FIG. 7. Charge density contour lines of the unoccupied states contributing to the tunneling current at low T along [001] in a logarithmic mesh. Upper panel: Contours along the Ti-rows showing Cl, lower panels: along the bridging O rows. The bold line corresponds to the experimental tip-sample distance.

than an O vacancy on a clean surface, compare, for example, the lower right panel in Fig. 7 with the lower left panel in Fig. 8.

Figure 8 displays the calculated STM line scans of the adsorption in an O vacancy. As already mentioned, O vacancies appear as bright spots along dark O rows on the clean surface (left box in the lower panel of Fig. 8). Replacing the O vacancy with Cl does not alter this feature significantly. According to the shape of the contours, the spots should appear smaller and more richly structured.

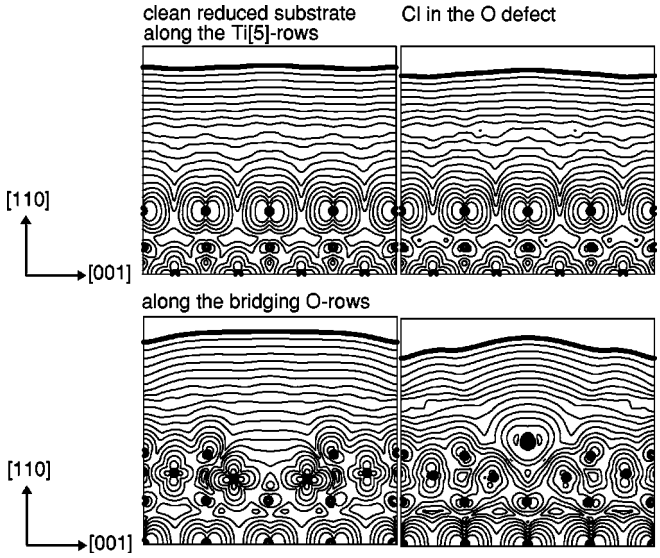

FIG. 8. Charge density contour lines of the unoccupied states contributing to the tunneling current at high T along [001] in a logarithmic mesh. Upper panel: Contours along the bridging O rows (showing Cl on the right panel), lower panels: along the bridging Ti rows. The left panels show the clean reduced surface. The bold line corresponds to the experimental tip-sample distance.

IV. DISCUSSION

A. Adsorption geometry and energetics

The experimentally observed adsorption geometries are a mixture of the configurations used in the calculations (Fig. 5). Adsorption at room temperature results in occupation of up to 40% of the $Ti^{[5]}$ atoms. Two different surfaces were prepared in the experiment: One where Cl was dosed on a slightly reduced surface, and one where the O vacancies were filled by exposure to molecular oxygen prior to the chlorine adsorption experiment.[49] The VB spectra of these two surfaces are practically indistinguishable from each other. The oxygen predosed surfaces are expected to resemble most closely the stoichiometric surfaces displayed in Figs. 5(a),(b), with the caveat that the dissociative adsorption of oxygen at a slightly defective surface might result in O adatoms, which can affect the adsorption of other molecules.[50,51] Experimentally, the slightly defective surface can be prepared in a more reliable way. However, in the *ab initio* calculations, only a high defect concentration of 25% could be considered for practical reasons.

Nevertheless, the comparison between calculated and experimental results shows a remarkably good agreement. According to the adsorption energies shown in Table II, the most favorable adsorption site should be an O vacancy. Also, the measured photoemission data in Fig. 2 and the experimental STM image in Figs. 1 and 3 suggest that oxygen vacancies, if present, are filled very rapidly with chlorine. The STM results after high-temperature adsorption are in agreement with the calculated results; adsorption at elevated temperature results in a massive replacement of bridging oxygen atoms. It has been pointed out in a recent publication[19] that a kinetic barrier prevents adsorbates from reaching these sites at room temperature. At elevated temperatures, oxygen vacancies and other defects within the bulk-reduced sample migrate to the surface and react with the Cl atoms that are weakly bound to the $Ti^{[5]}$ atoms. Ad-

sorption on bridge and top sites is energetically very similar[42] suggesting a high mobility of the Cl atoms in this precursor state.

According to the calculated data, the stoichiometric surface is far less reactive for Cl adsorption than the reduced one. Adsorption is less favorable by 2.5 eV per Cl atom if compared to adsorption on $Ti^{[5]}$ with a maximum Cl–O defect distance on the reduced surface in an (1×4) supercell [Fig. 5(d) and Table II]. This difference appears to be very large compared to the small differences in E^{ads} calculated for the different Cl configurations on a reduced substrate surface ($\leqslant 0.4$ eV), which seems to be surprising at first sight. However, one has to be aware that the size of the supercell along the $[1\bar{1}0]$ direction is very small. Especially the in-line adsorption geometry seems to be stabilized by the –Cl–○–Cl–○– chains. This stabilization is still present, though of slightly less importance, if Cl and the vacancies are arranged in zigzag geometry. Therefore, not only the O vacancy, but also the surrounding surface act as an ''activated region'' for the adsorption process. This might direct the Cl atoms moving along the Ti rows towards an O vacancy. A comparison to high-Cl coverage density calculations also shows that Cl seems to favor adsorption sites that maximize the number of vacancy sites in its neighborhood.[39]

B. Electronic structure

Because FLAPW is an all-electron method, core densities and energy levels are included into the electronic self-consistency procedure. The calculated energies of the Cl $p_{3/2}$ levels given in Table II can be qualitatively compared to the experimental XPS binding energies.[19] A binding energy of 199.4 eV was measured for adsorption at room temperature on the slightly defective surface, where a few Cl atoms fill O vacancies and most of them bind to $Ti^{[5]}$ atoms. That means that the experimental situation corresponds to some mixture of geometrical configurations like in Figs. 5(b),(d),(e),(f). The Cl $2p$ level increases by 0.4 eV when only O vacancies are occupied under high-temperature adsorption conditions as in Fig. 5(e) (ignoring Cl incorporation in the protrusions). No core-hole relaxations are included in the calculations. Hence, the calculated adsorption-induced core level shifts correspond to shifts of the initial states only. Furthermore, as the binding energies are measured with respect to the Fermi level in XPS, the differences of these two energies should also be taken into account when comparing experimental and calculated results. When applying this correction to the data in Table II, one obtains binding energies of 182.6 eV for Cl adsorbed on the stoichiometric surface and, rather independent of the actual adsorption site, 183.5 eV for Cl adsorbed on the reduced surface. The calculated shift of 0.9 eV towards higher binding energies is in reasonable agreement with the experimental value of 0.4 eV, given the drastic approximations made in the calculations.

A comparison between the photoemission spectra in Figs. 2 and 6 shows good agreement. The Ti $3d$ derived defect state, clearly visible as a separate peak in Fig. 2(a), is not split off from, but shifted to, the lower edge of the conduction band in Fig. 6(a). The reason may be that the antibonding levels are not lowered sufficiently to push the peak position into the gap if only a part of the Ti–O bonds are broken.[49,52] The replacement of bridging O atoms by Cl reduces the surface, which is reflected in the defect state in Fig. 2(d) and an increase in the Ti $2p$ shoulder in XPS. Similarly, the DOS and the calculated PES of a reduced surface also resemble those where Cl is occupying the O vacancies [Figs. 6(a),(b)]. When Cl is situated in an O vacancy and bound to two $Ti^{[6]}$, it hybridizes much stronger with substrate states than when adsorbed on a $Ti^{[5]}$ atom. This may cause the drastic change of the VB shape after high-temperature adsorption [Fig. 2(d)] as compared to a clean surface or one where most of the Cl is adsorbed at $Ti^{[5]}$. It is not surprising that the sharp Cl $3p$ peak in the DOS at the upper edge of the occupied states is not observed. The cross section for photoionization of atomic Cl states is very small,[32] and might be altered additionally when Cl interacts with the rutile substrate. The calculated ionization cross sections of the Cl $3p$ levels are significantly smaller than for the O $2p$ levels for Cl-covered TiO_2. Moreover, the LDOS in Fig. 6 exaggerate the intensity of this state because the shown total DOS is divided by a factor of 10.

Table II shows large differences in the work functions of the different surfaces. Note that the measured changes in work functions are referenced to a slightly defective surface. Upon adsorption of Cl the work functions are raised considerably, due to the enhanced electronegativity of the outermost Cl atoms. The experimentally determined increase of 0.5 eV for adsorption at elevated temperature should be compared with the difference of 1 eV between a clean, reduced surface and one where Cl fills all the oxygen vacancies. The concentration of O vacancies depends somewhat on the exact preparation conditions, but ranges typically around 5–10 %. The calculated work functions φ of the clean TiO_2 substrates depend significantly on the concentrations of O vacancies on the surface.[39] Changing the surface layer stoichiometry from Ti_4O_8 to Ti_4O_7 causes a drop of 2 eV in φ. The effect of further reduction to Ti_4O_6 is far less significant [$\Delta\varphi = -1.0$ eV (Ref. 39)]. Clearly, this strong dependence of the work function on the vacancy concentration prevents a more quantitative agreement with the experimental values.

C. Interpretation of STM images

The role of STM in revealing atomistic details relevant to surface adsorption and reaction mechanisms is undenied. However, image interpretation is not always straightforward, and the appearance of single individual atoms on flat surfaces is counterintuitive at times. In addition, the contrast of small adsorbates on metal surfaces may depend on the state of the tip.[53,54] Detailed calculations of the electronic structure help to unravel the appearance of adsorbed atoms on metal surfaces, as recently reviewed by Sautet.[55]

Constant-current topographies (CCT's) of the rutile TiO_2 (110) surface are dominated by electronic effects. The bridging oxygen atoms usually appear lower than the $Ti^{[5]}$ atoms, despite the fact that the former protrude by 1.2 Å above the surface. The reason for this lies in the negative polarity of the tip, which provides scanning of empty states that are largely

Ti 3*d* derived. Only very few empty O states are available for tunneling. However, adsorbed Cl atoms appear as bright features in empty-states STM images, independent of the state of the tip (Fig. 4). This is all the more surprising, as Cl is a very electronegative element for which very few empty states are expected. The calculated partial DOS in Fig. 6 supports this assumption.

The simple approach to the simulated STM images displayed in Figs. 7 and 8 does not include electron transition probabilities from tip to the sample, and neglects a variety of other factors, such as tip-sample forces, polarizabilities, etc. Nevertheless, a comparison of charge-density maps with experimental results gives good qualitative agreement of both the image contrast and appearance of the adsorbates. In the STM images, the Cl atoms cause a big, broad bump when bound to the $Ti^{[5]}$ atoms in an on-top geometry. While some of the broadening is probably tip induced, the much smaller appearance of the point defects in Fig. 1 indicates a sharp tip. The contours in Fig. 7 show that the Cl atom changes the density of states considerably over a relatively large area, and the LDOS in Fig. 6 indicate that the Ti 3*d* states are relevant for the tunneling current. These are mainly localized at Ti atoms involved in Cl–Ti bonding, i.e., the STM scans the altered Ti states rather than the Cl states themselves. An analysis of the LDOS at the CB edge[39] reveals that Ti atoms next to an O vacancy or a Cl adsorbate give the predominant contributions to the DOS in the STM-energy range. When Cl replaces a bridging O atom as in Fig. 5(e), its appearance resembles a missing O atom (Figs. 3 and 8, lower panels). Several other molecular and atomic adsorbates were investigated so far with STM, such as formate,[57] acetate,[56] pyridine[58] and its derivates,[59] benzoic acid,[60] S,[14–17] and Na.[61,62] They all appear bright in empty-states CCT's. It would be quite interesting to calculate how much of the image contrast is due to actual adsorbate states, and how much is due to Ti atoms, which are affected by the presence of the adsorbate.

V. SUMMARY

We investigated Cl adsorption on stoichiometric and reduced rutile TiO_2 (110) surfaces by experimental techniques (STM, PES, XPS) and an *ab initio* density functional method. The reduced surface was shown to be more active for adsorption. The calculated adsorption energies as well as the photoemission spectra indicate that Cl is preferably captured by oxygen vacancies. Alternative adsorption sites are the undercoordinated Ti at the surface. These two adsorption types show significant differences in work-function changes and the shifts of the Cl $p_{3/2}$ peaks. Generally, φ is increased upon Cl adsorption because of the large electronegativity of the protruding adsorbate species.

In empty-states STM images, adsorbed Cl atoms appear as wide bright spots. These bright spots can be addressed to unoccupied *d* states of the Ti atoms involved in adsorbate-substrate bonding rather than to the adsorbed Cl atoms, as also shown by the calculated local partial densities of states and line scans.

ACKNOWLEDGMENTS

This work was supported by the Austrian Science Foundation (D.V., project nr. T24-TPH) and an NSF-CAREER grant (Tulane) and the Center for Computational Materials Science (CMS) in Vienna. All calculations were performed on the NEC-SX4 supercomputer of the la server at the University of Technology in Vienna.

*Electronic address: Doris.Vogtenhuber@univie.ac.at

[1] D. Vogtenhuber, R. Podloucky, A. Neckel, S. G. Steinemann, and A. J. Freeman, Phys. Rev. B **49**, 2099 (1994).
[2] M. Ramamoorthy, R. D. King-Smith, and D. Vanderbilt, Phys. Rev. B **49**, 16 721 (1994).
[3] M. Ramamoorthy, D. Vanderbilt, and R. D. King-Smith, Phys. Rev. B **49**, 7709 (1994).
[4] N. M. Harrison, X. G. Wang, J. Muscat, and M. Scheffler, Faraday Discuss. **114**, 305 (1999).
[5] P. J. D. Lindan, N. M. Harrison, M. J. Gillan, and J. A. White, Phys. Rev. B **55**, 15 919 (1997).
[6] S. P. Bates, G. Kresse, and M. J. Gillan, Surf. Sci. **385**, 386 (1997).
[7] Y. Iwasawa, H. Onishi, and K. Fukui, Bull. Chem. Soc. Jpn. **68**, 2447 (1995).
[8] *Oxide Surfaces*, Vol. 9 in The Chemical Physics of Solid Surfaces, edited by D. P. Woodruff (Elsevier, Amsterdam, 2001).
[9] U. Diebold, J. F. Anderson, K. O. Ng, and D. Vanderbilt, Phys. Rev. Lett. **77**, 1322 (1996).
[10] G. Charlton *et al.*, Phys. Rev. Lett. **78**, 495 (1997).
[11] B. Hird and R. A. Armstrong, Surf. Sci. **420**, L131 (1999).
[12] G. N. Raikar, P. J. Hardman, C. A. Muryn, G. van der Laan, P. L. Wincott, G. Thornton, and D. W. Bullett, Solid State Commun. **80**, 423 (1991).
[13] C. N. Satterfield, *Heterogeneous Catalysis in Industrial Practice* (McGraw-Hill, New York, 1991).
[14] E. L. D. Hebenstreit, W. Hebenstreit, and U. Diebold, Surf. Sci. **461**, 87 (2000).
[15] E. L. D. Hebenstreit, W. Hebenstreit, and U. Diebold, Surf. Sci. **470**, 347 (2001).
[16] E. L. D. Hebenstreit, W. Hebenstreit, H. Geisler, C. A. Ventrice, Jr., P. T. Sprunger, and U. Diebold, Surf. Sci. **486**, L467 (2001).
[17] E. L. D. Hebenstreit, W. Hebenstreit, H. Geisler, C. A. Ventrice, Jr., D. Hite, P. T. Sprunger, and U. Diebold, Phys. Rev. B (to be published).
[18] U. Diebold, W. Hebenstreit, G. Leonardelli, M. Schmid, and P. Varga, Phys. Rev. Lett. **81**, 405 (1998).
[19] E. L. D. Hebenstreit, W. Hebenstreit, H. Geisler, C. A. Ventrice, Jr., P. T. Sprunger, and U. Diebold (unpublished).
[20] V. E. Henrich and P. A. Cox, *The Surface Science of Metal Oxides* (Cambridge University Press, Cambridge, 1994).
[21] H. Onishi, K. Fukui, and Y. Iwasawa, Colloids Surf., A **109**, 335 (1996).
[22] R. A. Bennett, P. Stone, R. Smith, and M. Bowker, Surf. Sci. **454-456**, 454 (2000).
[23] K.-O. Ng and D. Vanderbilt, Phys. Rev. B **56**, 10 544 (1997).
[24] O. Gülseren, R. James, and D. W. Bullett, Surf. Sci. **377-379**, 150 (1997).

[25] W. Heegeman, K. H. Meister, E. Bechtold, and K. Hayek, Surf. Sci. **49**, 161 (1975).
[26] U. Diebold, H.-S. Tao, N. D. Shinn, and T. E. Madey, Phys. Rev. B **50**, 14 474 (1994).
[27] R. L. Kurtz, R. Stockbauer, T. E. Madey, E. Roman, and J. L. de Segovia, Surf. Sci. **218**, 178 (1989).
[28] E. Bertel, R. Stockbauer, and T. E. Madey, Phys. Rev. B **27**, 1939 (1983); Surf. Sci. **152/153**, 776 (1985).
[29] M. A. Henderson, W. S. Epling, C. L. Perkins, C. H. F. Peden, and U. Diebold, J. Phys. Chem. B **25**, 5328 (1999).
[30] E. M. Snigiryova, S. I. Troyanov, and V. B. Rybakov, Zh. Neorg. Khim. **35**, 1945 (1990).
[31] K. Dehnicke, Z. Anorg. Allg. Chem. **309**, 266 (1961).
[32] J. J. Yeh and I. Lindau, At. Data Nucl. Data Tables **32**, 1 (1985).
[33] M. A. Henderson, Surf. Sci. **355**, 151 (1996).
[34] P. J. Hardman, G. N. Raikar, C. A. Muryn, G. van der Laan, P. L. Wincott, G. Thornton, D. W. Bullett, and P. A. D. M. A. Dale, Phys. Rev. B **49**, 7170 (1994).
[35] H. Krakauer, M. Posternak, and A. J. Freeman, Phys. Rev. B **19**, 1706 (1979); M. Posternak, H. Krakauer, A. J. Freeman, and D. D. Koelling, *ibid.* **21**, 5601 (1980); E. Wimmer, H. Krakauer, M. Weinert, and A. J. Freeman, *ibid.* **24**, 864 (1981).
[36] P. Hohenberg and W. Kohn, Phys. Rev. **136**, B864 (1964); W. Kohn and L. J. Sham, *ibid.* **140**, A1133 (1965).
[37] L. Hedin and B. I. Lundqvist, J. Phys. C **4**, 2064 (1971); L. Hedin and S. Lundqvist, J. Phys. (France) **33**, C3 (1972).
[38] G. Lehmann and M. Taut, Phys. Status Solidi B **54**, 469 (1972).
[39] D. Vogtenhuber, R. Podloucky, and J. Redinger (unpublished).
[40] R. Yu, D. Singh, and H. Krakauer, Phys. Rev. B **43**, 6411 (1991).
[41] A. Di Pomponio, A. Continenza, R. Podloucky, and J. Vackar, Phys. Rev. B **53**, 9505 (1996).
[42] D. Vogtenhuber, R. Podloucky, and J. Redinger, Surf. Sci. **454-456**, 369 (2000).
[43] J. Tersoff and D. R. Hamann, Phys. Rev. B **31**, 805 (1985); J. Tersoff, *ibid.* **41**, 1235 (1990); **40**, 11 990 (1989).
[44] J. Redinger, P. Marksteiner, and P. Weinberger, Z. Phys. B: Condens. Matter **63**, 221 (1986).
[45] J. Redinger, J. Yu, A. Freeman, and P. Weinberger, Phys. Lett. A **124**, 463 (1987).
[46] These relaxations, in particular $Ti^{[6]}$ and O(plane) differ from our previous result,[1] which might be due full convergence of basis sets and the implementations of forces.[41] The present results are in good agreement with,[2] although the mixed surface plane is slightly closer to the bulk in our calculations.
[47] J. Redinger *et al.* (unpublished).
[48] P. W. Atkins, *Physical Chemistry*, 2nd ed. (W. H. Freeman, San Francisco, 1982).
[49] D. Vogtenhuber, R. Podloucky, J. Redinger, W. Hebenstreit, and U. Diebold (unpublished).
[50] M. A. Henderson, W. S. Epling, C. L. Perkins, C. H. F. Peden, and U. Diebold, J. Phys. Chem. B **103**, 5328 (1999).
[51] W. S. Epling, C. H. F. Peden, M. A. Henderson, and U. Diebold, Surf. Sci. **412/413**, 333 (1998).
[52] J. Redinger and P. Weinberger, Phys. Rev. B **35**, 5652 (1987).
[53] L. Ruan, F. Besenbacher, I. Stensgaard, and E. Laegsgaard, Phys. Rev. Lett. **70**, 4079 (1993).
[54] L. Bartels, G. Meyer, and K.-H. Rieder, Surf. Sci. Lett. **432**, L621 (1999).
[55] P. Sautet, Chem. Rev. **97**, 1097 (1997).
[56] H. Onishi, Y. Yamaguchi, K. Fukui, and Y. Iwasawa, J. Phys. Chem. **100**, 9582 (1996).
[57] H. Onishi and Y. Iwasawa, Chem. Phys. Lett. **226**, 111 (1994).
[58] S. Suzuki, Y. Yagamuchi, H. Onishi, K. Fukui, T. Sasaki, and Y. Iwasawa, Catal. Lett. **50**, 117 (1998).
[59] S. Suzuki, Y. Yagamuchi, H. Onishi, K. Fukui, T. Sasaki, and Y. Iwasawa, Catal. Lett. **54**, 177 (1998).
[60] Q. Guo, I. Cocks, and E. M. Williams, Surf. Sci. **393**, 1 (1997).
[61] P. W. Murray, N. G. Condon, and G. Thornton, Surf. Sci. **323**, L281 (1995).
[62] H. Onishi and Y. Iwasawa, Catal. Lett. **38**, 89 (1996).